Renewable Energy 239 (2025) 122054

Contents lists available at ScienceDirect

Renewable Energy

journal homepage: www.elsevier.com/locate/renene

Optimisation of Luminescent Solar Concentrators through an Integrated Optical & Electrical Model

Aaron Glenn [a,*], Subhash Chandra [b], Mojtaba Nasiri [a], Sarah McCormack [a]

[a] Civil, Structural & Environmental Engineering, Trinity College Dublin, Dublin, D02 PN40, Ireland
[b] Department of Geology, School of Natural Sciences, Trinity College Dublin, Dublin, D02 PN40, Ireland

ARTICLE INFO

Keywords:
Optical modelling
Electrical modelling
Model validation
Simulations
Fabrication
Optimisation
Characterisation
Performance analysis
Building integrated photovoltaics

ABSTRACT

Luminescent and Plasmonic Luminescent Solar Concentrators (LSCs and PLSCs) represent significant advancements in solar energy utilisation. This paper introduces and validates a novel, comprehensive two–stage integrated model for optimising and evaluating the performance of these solar concentrating devices. The first stage, termed 'Plasmon' is an optical model that systematically optimises the optical characteristics of LSCs and PLSCs. Initially, the optical processes within LSCs were modelled and validated against laboratory–fabricated devices. This validation process was repeated for PLSC simulations ensuring congruence between the modelled and experimental results. Subsequently, the optical model was used to simulate various dye concentrations within LSCs of dimensions $10 \times 10 \times 0.5$ cm of which the optimal outputs were fabricated in the lab and tested in both indoor and outdoor environments. The second stage is a novel electrical model developed to predict and evaluate the outdoor performance of the LSC and PLSC devices. The electrical model incorporates the LSC & PLSC optical parameters & dimensions, as well as the direct and diffuse components of the solar radiation spectrum to simulate the devices electrical performance. The role of the electrical model is to predict key performance metrics of power output and power conversion efficiency, thereby providing a comprehensive evaluation of the devices. Comparative analysis shows that the model demonstrates a high degree of accuracy ($> 90\%$). This validated novel comprehensive model emerges as a powerful and versatile tool capable of accurately simulating diverse LSC & PLSC device configurations, dye types, and concentrations across various environmental and seasonal conditions. It offers significant material, time, and cost savings in the research and development of these technologies.

1. Introduction

Greenhouse gas (GHG) emissions, especially those of carbon dioxide (CO_2) and methane (CH_4), contribute significantly to global warming through the trapping of heat in the atmosphere [1–4]. The concentration of CO_2 in the atmosphere is increasing at an alarming rate, reaching 427 ppm in 2024 [5]. As of 2022, approximately 80% of the world's energy production relied on fossil fuels, primarily coal, oil, and gas and this heavy dependence on fossil fuels, coupled with emissions from cement production, resulted in an output of 36.6 billion tonnes of CO_2 into the atmosphere in just one year [6,7].

The building sector alone accounts for nearly one third of all global energy consumption, with the built environment being responsible for 40% of Europe's energy usage. This sector is also responsible for 36% of Europe's total greenhouse gas emissions, and 28% of GHGs globally [8].

One vital approach in our effort to reduce our GHG emissions is the large–scale adoption of renewable energy technologies to combat our reliance on fossil fuel resources. Research, development, and implementation of solar, hydro, and wind technologies for example will be crucial to building a sustainable future [9–11]. Overall, renewable energy technologies emit between 400–1000 g of CO_2 equivalent per kWh less than their fossil fuel counterparts which lack carbon capture [12]. This paper focuses on one such renewable energy technology: the Luminescent Solar Concentrator (LSC), a solar radiation concentrating device used to generate cleaner power.

Luminescent solar concentrators (LSCs) are optical devices that can enhance the performance of photovoltaic (PV) cells by concentrating and redirecting the incoming solar radiation to the active area of the photovolatic (PV) cells [13]. LSCs are essentially transparent waveguides that are doped with luminescent materials, such as organic dyes [14], quantum dots [15,16], or rare earth ions [17], which can absorb photons and re–emit them at longer wavelengths. The re–emitted photons are then trapped within the waveguide via total internal reflection (TIR), and are directed towards the edges of the waveguide

* Corresponding author.
E-mail address: aglenn@tcd.ie (A. Glenn).

https://doi.org/10.1016/j.renene.2024.122054
Received 22 August 2024; Received in revised form 29 October 2024; Accepted 28 November 2024
Available online 5 December 2024

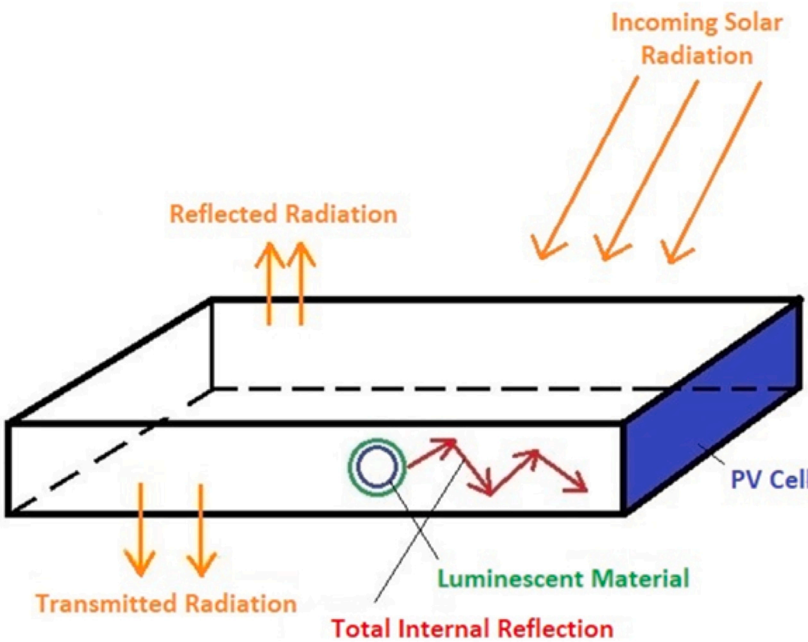

Fig. 1. Schematic diagram of the operating principles of an LSC [18].

where the PV material is located. This design and waveguiding process is displayed diagrammatically in Fig. 1.

First proposed in the early 1970's [19], the luminescent materials used in the devices can have tailored absorption and emission spectra which allows them to absorb a wide wavelength range, convert them to lower–energy photons and efficiently transport them within the waveguide. The thickness, surface area, and the refractive index of the waveguide as well as the doping concentrations of the luminescent particles are all critical parameters that affect the optical performance of the LSC.

There have been constant efforts to improve LSC performance with research being conducted on the quantum dot LSC (QDLSC) [20,21], the rare earth doped LSC [22], and the plasmonic LSC (PLSC) [23,24] with the hopes of enhancing the photon transfer to the PV cells. An LSC becomes a PLSC whenever the waveguide is doped with a plasmonic element like a metal nanoparticle (MNP) to enhance the optical efficiency of the luminescent material species [18]. A metal nanoparticle is, by definition, a particle of size within the 1–100 nm range and are of interest due to their ability to collectively excite conductive band electrons which exhibit extraordinary plasmonic optical properties [25]. These properties include the enhanced photon mode density through the concentration of optical energy in the sub–wavelength range in a phenomenon referred to as localised surface plasmon resonance (LSPR). The plasmonic interactions between the enhanced photon mode density and the luminescent materials can modify the optical properties of these luminescent particles and as a result improve the optical performance of the PLSC. The MNPs used in LSCs usually consist of gold (Ag) and silver (Au) due to;

- Their scattering and extinction peaks are within the desired wavelength range (300–900) [26]
- Their optical properties are tuneable via altering the particles geometry [27]
- They are stable over long periods of time [28]

Gold–core, silver–shell MNPs are included in this study to induce this LSPR phenomenon within the waveguide to further enhance the layers ability to absorb and emit photons so that more energy reaches the PV cells. It has been reported that LSPR can increase the devices' outputs by a factor of 1.4–2.3 times when compared to an LSC [24].

The optimisation of the LSC & particularly the PLSC devices proves to be challenging due to the complicated interplay between the optical and electrical processes. There have been various optical models developed which assist with the optimisation of the LSC device parameters however no model so far has been able to combine the optical simulations paired with plasmonics with an electrical model capable of predicting LSC power output and power conversion efficiencies [14,29–31]. This study aims to address this challenge by presenting a novel comprehensive model that has the ability to accurately simulate all of these processes within the devices. The outcome is a verified model capable of simulating various device configurations and dimensions, dye types and concentrations, as well as different metal nanoparticle types and concentrations in real world conditions in terms of both their optical characteristics as well as their outdoor electrical performance.

2. Materials & methods

This paper establishes and validates a comprehensive model for LSCs in two stages. Initially, the optical model is tested and validated, and subsequently used to optimise the LSC and PLSC devices for performance analysis in both indoor and outdoor environments. Following this, electrical performance simulations are conducted and compared with the outdoor experimental recordings, using only the day–specific solar radiation data, the configuration of the device and the external photon efficiency taken from the optical model as inputs. External photon efficiency and optical efficiency are used interchangeably in this study to mean the ratio of photons from solar radiation entering the LSC that reach the PV cells, accounting for both optical losses and re-emission processes [32].

2.1. The model

The optical model developed by the Solar Energy Applications Group (SEAG) at Trinity College Dublin and validated in this study is an advanced approach designed to simulate the complex optical and plasmonic interactions within LSC and PLSC layers [33]. Integrating a ray tracing algorithm with an optimised three–dimensional finite difference time domain (OFDTD) approach, the model offers high precision in replicating photon–level behaviour across varying material properties, dye concentrations, and device configurations. This

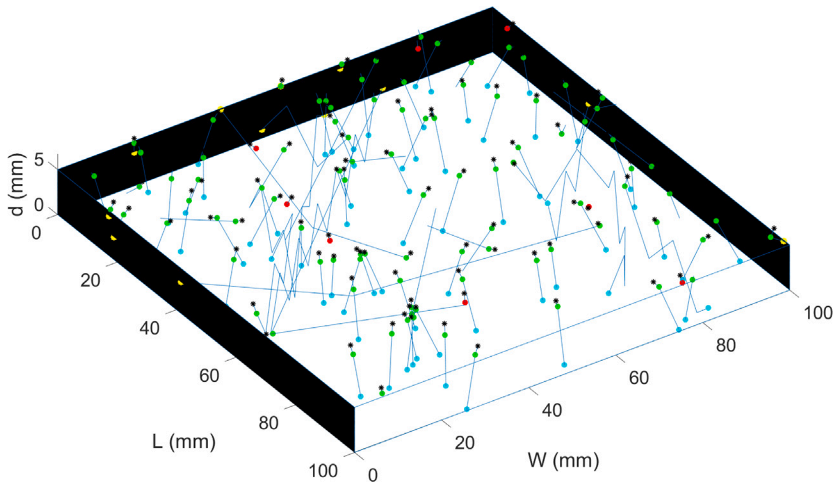

Fig. 2. Monte Carlo ray tracing simulating the outcome of each incoming photon. Black asterisk' denote the input source of the photon, green dots indicate the point at which the photons first intersect with the layer, red dots depict photons lost through thermal mechanisms, cyan dots depict optical losses and yellow dots display photons that reach the PV cell.

model aims to improve light–harvesting efficiency in customised LSC designs by enabling accurate predictions of optical behaviour at both macroscopic and microscopic scales.

Traditional ray-tracing approaches bring several significant advantages:

- **High–Resolution Modelling:** Traditional ray–tracing offers precise, photon–level interactions based on physical principles, modelling key phenomena which directly impact LSC efficiency.
- **Validation and Predictive Strength:** Ray–tracing can be validated against experimental data to achieve predictive accuracy in varying configurations, dye concentrations, and device dimensions. This is a significant advantage when working with well–defined device parameters.
- **Adaptability to Complex Structures:** Unlike methods that rely on historical data, ray tracing can be applied to novel LSC geometries and luminescent materials, making it a valuable tool for innovative device structures.

As a complementary or alternative approach, recent developments in AI and machine learning offer faster processing speeds and generalisation capabilities. However, these methods depend on high-quality training data and lack transparency regarding photon-level interactions, which may limit their precision in certain applications [34].

The Monte Carlo Ray Tracing (MCRT) algorithm, central to this model, uses a probabilistic approach to track photon behaviours through the LSC. It accurately simulates loss mechanisms including reflection, refraction, absorption, scattering, attenuation, wave–guiding, and transmission, predicting the likelihood of photons reaching the PV cells at the device edges. Fig. 2 visually demonstrates this ray tracing process, where individual photon paths and interaction points are traced to capture the overall light-harvesting efficiency of the device.

The simulation was conducted on LSCs made from a polydimethylsiloxane (PDMS) host matrix, positioned atop a glass substrate with silicon PV cells positioned along all four edges. The algorithm generates a number of rays limited to a maximum of approximately 200,000 rays in this study due to the hardware limitations of the computer. Each of these rays then undergo a series of possible optical events listed above dependent on the weighted probability from the materials properties and the characteristics of the incoming ray. The model uses a random number generator associated with these respective probabilities to determine which event occurs and which rays ultimately reach the PV cells at the edges of the device. This study used a 4–edge PV cell configuration with a reflective backplate on the device for each of the simulations for comparative purposes. The reflector used in this study was a 3M^{TM} Daylighting Film DF2000MA reflective film with a luminous reflectivity of >99% implemented with an air gap to ensure TIR.

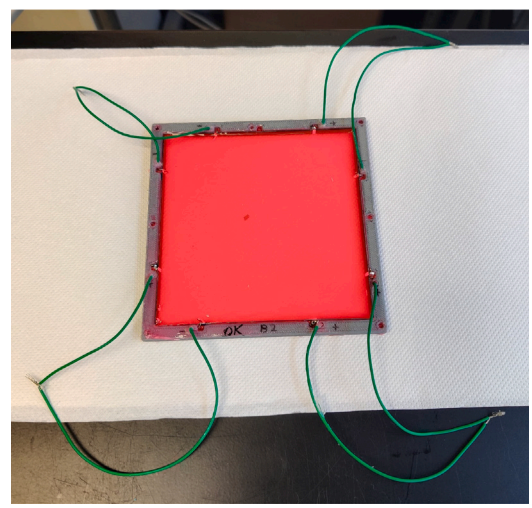

Fig. 3. Lab fabricated LSC.

Fig. 3 displays a lab fabricated LSC on which these simulations are based. The fabrication technique can be found in previous work [35]. The silicon solar cells used in this study came from DMEGC, with an efficiency of 22%. The standard operating parameters are a nominal operating cell temperature (NOCT) of $42 \pm 3\,^{\circ}C$ and temperature coefficient of $-0.330\%/^{\circ}C$. However, due to LSC panel fabrication and electrical connection difficulties, only one bus bar from the front and rear of the solar cell was used for the electrical connections, which reduces the efficiency to 14%. The solar cells were cut to 100×10 mm and 50×10 mm by SunWare GmbH. The silicon PV cells have been modelled using a standard one–diode–model (ODM).

With regards to simulating the plasmonic effects within a PLSC, the OFDTD model operates in 3 stages;

- *Pre–processing* –Inputs defined in Fig. 4 are applied, this in turn designs the Yee grid, boundary conditions, simulation time intervals, any constant variables and constitutive relations [36].
- *Main Loop* –Maxwell's equations are solved using a leapfrog process, in which the electrical field is solved at one instant and the

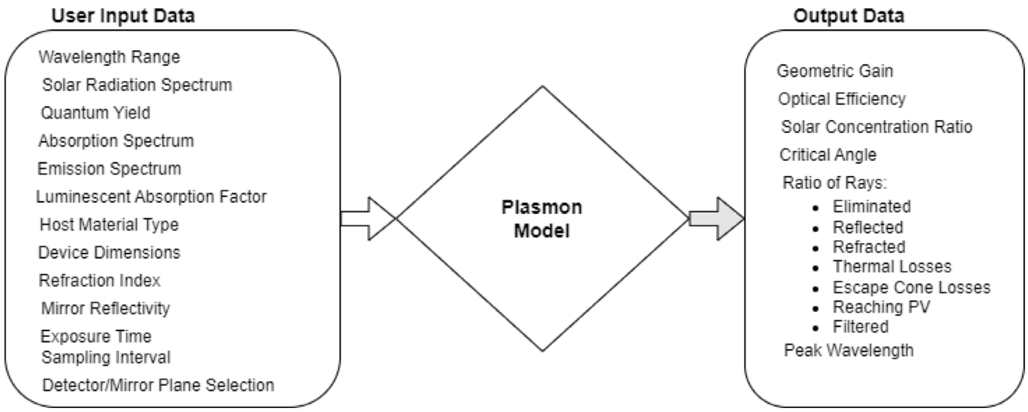

Fig. 4. Inputs required for plasmonic model along with resulting outputs.

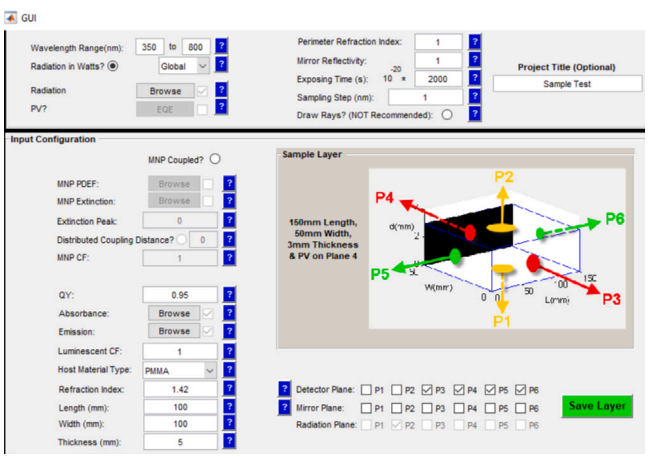

Fig. 5. Graphical user interface of modelling software.

magnetic field updated and solved at the next time instant [37]. Conditional statements accounting for the probability of attenuation, absorption, scattering and transmission are implemented with the highest probability being prioritised. Curl terms are integrated over the grid relative to the change in electric or magnetic field.

- *Post–processing* –This stage reduces the required memory from the PC as it bypasses any identical or repetitive calculations

These plasmonic simulations also take into consideration other possible energy loss mechanisms such as thermal re–absorption, energy quenching, and host material attenuation losses which result in a non–unity quantum yield (QY).

Fig. 4 details the inputs and outputs of the plasmonic model. The graphical user interface (GUI) of the model is also included in Fig. 5.

The additional inputs required for PLSC simulations are as follows;

- Metal Nanoparticle (MNP) Photon Density Enhancement Factor Spectrum
- MNP Extinction Spectrum
- MNP Extinction Peak
- MNP Concentration Factor

The third stage in the modelling process, the *post–processing* stage, returns the enhancement, output emission spectra, energy conversion efficiency parameters, total energy losses, and total thermal losses of the device in an excel spreadsheet.

Fig. 6 presents a schematic of the inputs required for the electrical model. This model requires information relating to the configuration of the LSC, the optical efficiency from the optical model and the solar radiation separated into total and diffuse components in order to make predictions of the LSC power output and power conversion efficiency.

Fig. 7 is included as a flow chart to help clarify this validation process for the comprehensive optical and electrical model.

2.2. Optical model validation

2.2.1. LSC optical modelling validation

Using the inputs in Fig. 5, the model was used to simulate the outputs of an LSC of dimensions of 45 mm × 45 mm × 3 mm with varying concentrations of the dye Lumogen F Red 305 ranging between 10–300 ppm. The wavelength range was 350–800 nm aligning with the spectrum region for the dye & silicon PV cells used in this study. These dimensions were selected as they could be compared with layers that had previously been fabricated [38]. The aim was to compare lab–fabricated layers with simulations to analyse the model's accuracy [39].

The layers were fabricated and their absorption and emission spectra measured using a BLK–C–SR–50 Concave Grating Spectrometer (StellarNet) connected to a 6–inch integrating sphere (RT–060–Sf Labsphere) illuminated by a DH–2000–BAL UV–VIS–NIR light source (Ocean Optics) not only for comparison purposes but also to feed the source data into the model. A conservative 95% quantum yield has

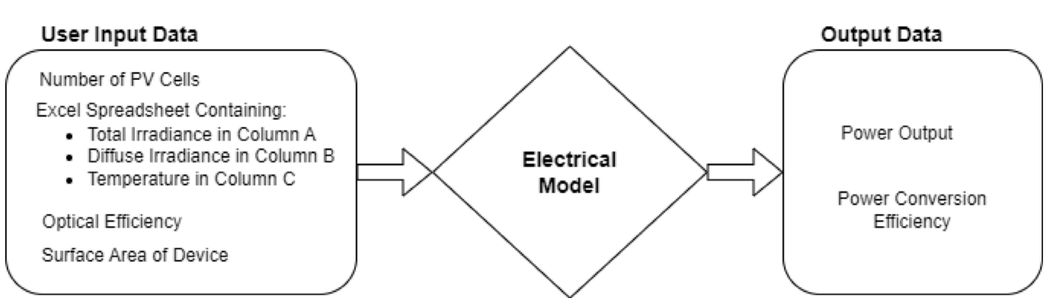

Fig. 6. Inputs required for electrical model along with resulting outputs.

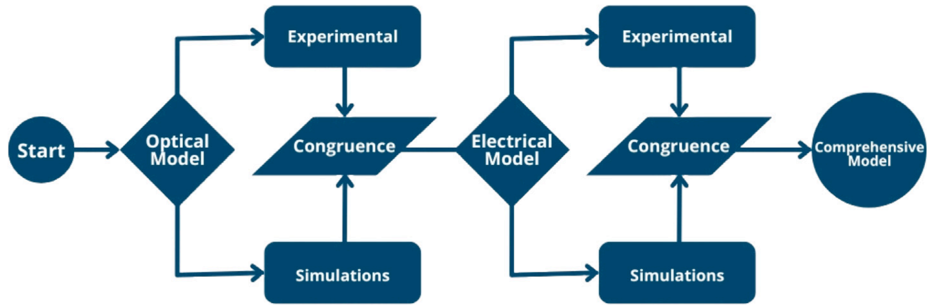

Fig. 7. Comprehensive model validation process.

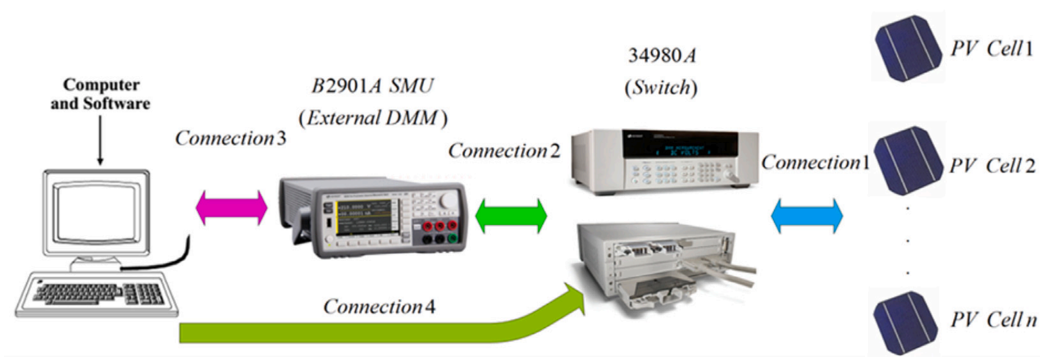

Fig. 8. Outdoor testing setup.

been used in this study even though there is evidence published that the Lumogen Red dye has a 97% quantum yield when mixed with PMMA [37]. The dimensions were input to match the layer fabricated in the lab, with a mirror reflectivity of 99% being included and the amount of rays set to 203,000 as this was the upper limit of the computers hardware capabilities.

2.2.2. PLSC optical modelling validation

This stage required additional input data specifically related to the metal nanoparticles (MNPs). This validation was performed after the simulations for LSC layers had been analysed and validated (see Figs. 9 through 11). The MNPs used in this study were gold–core, silver–shell nanocuboids synthesised in the lab [24,40,41]. The concentration of the dye was optimised at 70 ppm and as a result, the doping of the MNPs was set at a saturated point optimised through an iterative modelling and experimentation until a peak optical efficiency was determined. This test meant that the MNP extinction spectrum and peak had been obtained and that the only remaining variable to locate was the photon density enhancement factor (PDEF). The PDEF was obtained from an established dataset taken from a literature review that was originally used in the development of the plasmon model [33,42].

2.3. Electrical model validation

2.3.1. Outdoor data collection

This study extends previous LSC modelling validation by simulating the power output and power conversion efficiencies of the LSCs in real–world conditions validated by outdoor experimental data. A novel Visual Basic (VB) script was developed for collecting experimental outdoor data recording from a setup containing a B2901A Source Measurement Unit (SMU) and a 34980A Multifunction Switch/Measure Unit as shown in Fig. 8. These devices are linked to a PC with Visual Basic, Agilent's IO Libraries Suite, Keysight Connection Expert and Microsoft Office software installed. The visual basic scripts process a standard commands for programmable instruments (SCPI) language in order to synchronise the devices to take current and voltage measurements of the different LSC, PLSC and reference devices. The solar radiation data is recorded using a separate BF5 Sunshine Sensor device which was also attached to the outdoor panel alongside the LSC devices. This device is capable of measuring direct and diffuse solar radiation.

A secondary separate Visual Basic (VB) script then takes these experimental readings and converts the data into power outputs and power conversion efficiency readings in a time interval selected by the user. VB scripts are capable of taking readings over a large range of voltages and currents over a long period of time whilst also being adjustable to taking quick measurements of different device configurations.

2.3.2. Electrical modelling validation

In order to comprehensively validate the model, the final stage of the electrical performance of the simulations had to be verified through comparisons with simulation and experimental results. The electrical model has been developed using MATLAB software and as discussed previously requires the information regarding number of PV cells, solar radiation, surface area of the device, and the optical efficiency (see Fig. 6). Simulations were performed using the solar radiation data recorded experimentally and the optical efficiency from the plasmon model. The results of the simulations were compared with the experimentally recorded data and are included in the results section.

3. Results & discussion

3.1. Optical model validation & the optimisation of the PLSC

Fig. 9 shows the change in the devices' optical outputs when the Lumogen Red 305 dye concentration is varied. Figs. 9(a) & 9(b) depict the changing optical efficiency and solar concentration ratio as output by the optical model whereas Fig. 9(c) displays the edge emission recorded experimentally. Here, the optical model has simulated the

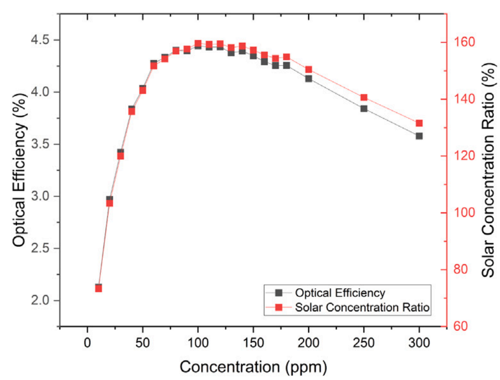

(a) Optical Efficiency and Solar Concentration Ratio of a 1 Edge PV Cell LSC Simulation vs Dye Concentration of Lumogen Red 305

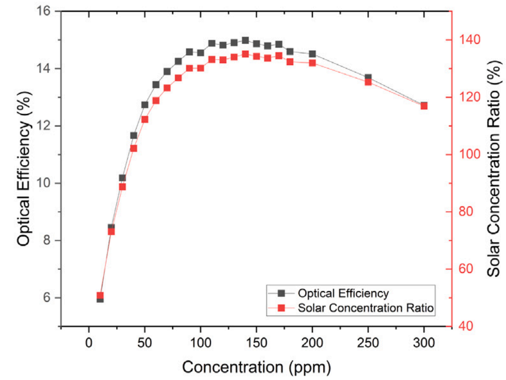

(b) Optical Efficiency and Solar Concentration Ratio of a 4 Edge PV Cell LSC Simulation vs Dye Concentration of Lumogen Red 305

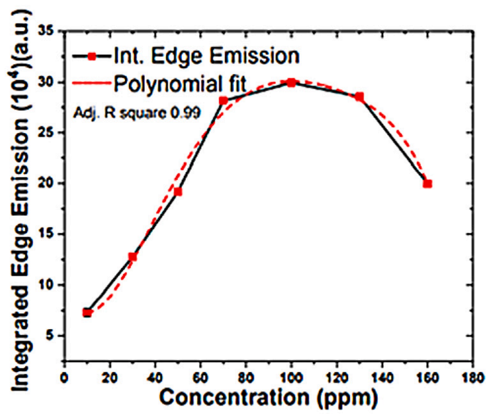

(c) Emission vs Lumogen Red 305 Dye Concentration Experimentally Measured (Sethi et al., 2022)

Fig. 9. Comparison of model output with experimental output using the optical plasmon model.

optical efficiencies and the solar concentration ratios of an LSC layer of dimensions 45 mm × 45 mm × 3 mm and the results of these simulations are compared with the experimental outputs of the same dimension layer measured in the lab. It is established from these results, that whilst the output is in terms of emission for the experimental results and optical efficiency for the simulations, the measurements are studying the same overall effect and the results correlate with a peak efficiency at approximately 70 ppm. This correlates with results found in a separate Monte Carlo ray tracing model study where an optimal Lumogen F Red 305 of 110 ppm has been observed in a different device configuration using bifacial PV cells [43].

Following validation of the optical model, which demonstrated a high degree of accuracy in replicating laboratory results, simulations were conducted to optimise the configuration of the LSC device. Fig. 10 details the results of the simulations performed in order to calculate the optimal lightguide thickness within a LSC device, thicknesses of 3, 5, 7 & 9 mm have been modelled. The use of an optimal dye concentration of 70 ppm has remained constant throughout these simulations with an observation that an increase of layer thickness leads to increased optical efficiencies. This increase in thickness leads to lower solar concentration ratios however as shown in the secondary Y-axis in the same graph. Increasing the LSC thickness also introduces higher thermal losses as detailed in Table 1, therefore 5 mm was used as it had the best overall predicted outputs after all loss mechanisms were considered.

Fig. 11 shows the results of simulations comparing surface area with optical efficiency and solar concentration ratio. It is clear that increasing the surface area of the LSC layer improves the solar concentration ratio but worsens the optical efficiency of the device. An optimal layer size of 100 cm^2 was selected for fabrication as it lies within the optimal range of 100–120 cm^2 as indicated in Fig. 11 where the two variables intersect as surface area varied. These dimensions are expected to allow the maximum amount of solar radiation to reach the PV cells.

Table 1
Thermal losses as thickness of LSC increases, all tested at a Lumogen Red 305 dye concentration of 70 ppm.

Thickness (mm)	Thermal losses (%)
3	7.6
5	8.4
7	9.4
9	10.2

The following set of results detail the validation process of the PLSC section of the optical model using the additional set of parameters required as discussed previously. Fig. 12(a) shows the experimentally measured extinction spectrum of the gold–core, silver–shell nanocuboids with Fig. 12(b) displaying the 10 ppm concentration spectrum used for fabrication. This graph represents the optimal finding, as the spectra were subdivided to determine the optimal concentration of MNPs after accounting for all variables. The photon density enhancement factor (PDEF) was the final variable required to simulate PLSC devices, it was taken from the literature [33] that was originally used to develop this model (Fig. 13(a)). The finalised PDEF for the Gold–core Silver–shell nanocuboids is shown in Fig. 13(b). The extinction spectrum was divided in order to find the optimal MNP concentration for

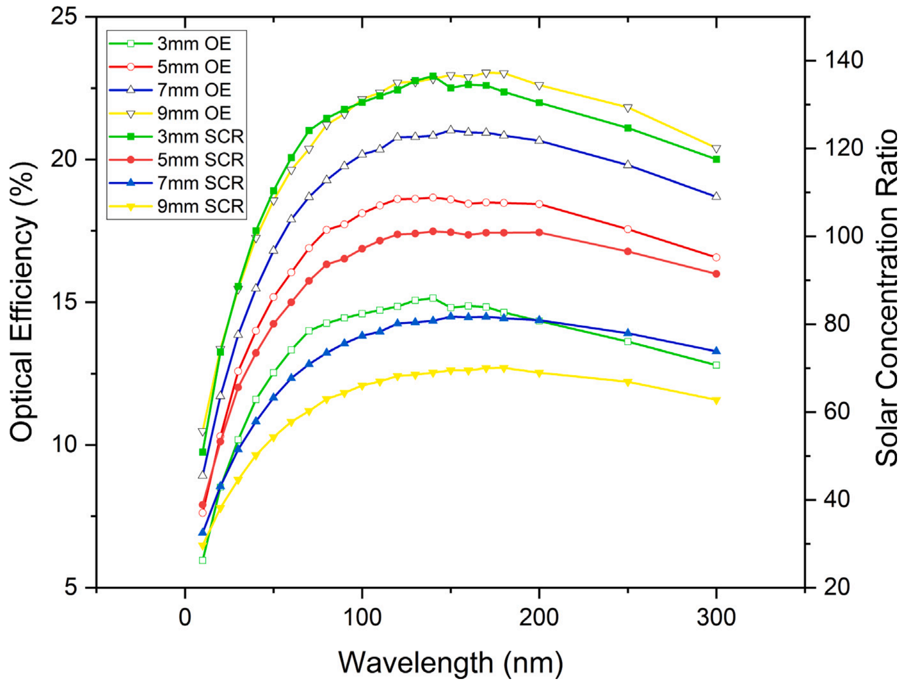

Fig. 10. Comparison of LSC thickness vs. the optical efficiency and solar concentration ratio.

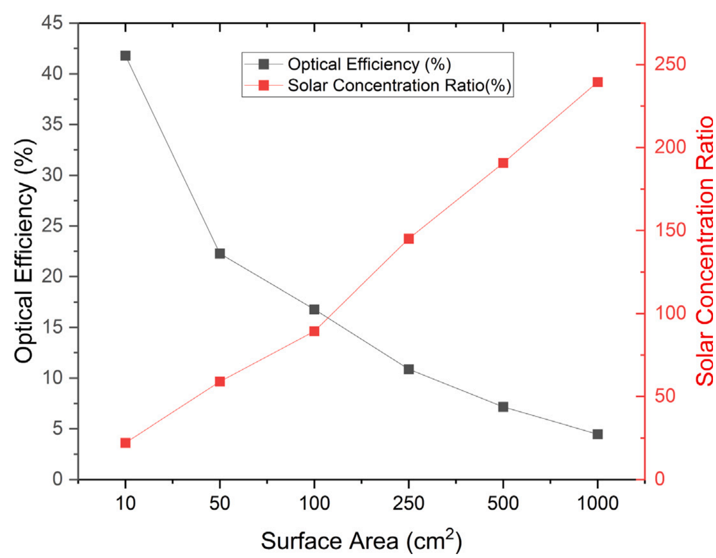

Fig. 11. Optical efficiency and solar concentration ratio vs. Layer surface area.

use in the already optimised LSC layer containing 70 ppm Lumogen Red 305 dye. The original measurement at 100 ppm was divided into various subdivisions with simulations run for each result, this is included in Fig. 14(a) where a concentration of 10 ppm was deemed optimal. Through comparisons with experimental measurements detailed in Fig. 14(b), the optical Plasmon model was deemed validated due to its accurate prediction of the results observed in the lab.

3.2. Outdoor data & electrical model validation

The validated optical model was used to optimise LSCs for fabrication & performance testing in real world conditions. The optimal layer is a 100 mm × 100 mm × 5 mm layer doped with 70 ppm Lumogen Red dye 305. For PLSC layers, an inclusion of a 10 ppm concentration of gold–core, silver–shell nanocuboids has been determined.

Fig. 15 displays a finding observed using the optical Plasmon model in which the LSC devices have been noted to perform more efficiently in terms of their power outputs and power conversion efficiencies when situated in highly diffuse solar irradiation environments. This ratio of enhanced performance is 1.76 times enhancement as the diffuse component becomes dominant. Interestingly, through analysis of the experimental data, a value of 1.763 has been noted as an under–estimation value for our model across multiple days of data when averaged out. As a result of this finding, a factor of this value has been built into the model for when the diffuse component is above 55% as well as a value of 0.786 for when the diffuse component is below 5%. These 'coefficients' have been applied equally to all data sets recorded in order to ensure accuracy across various conditions.

The optimised layers according to the model have been fabricated and tested in both indoor and outdoor conditions alongside the

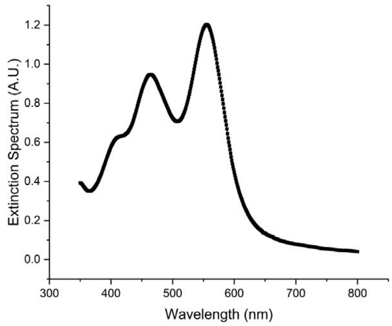

(a) Extinction Spectrum of Gold–Core Silver–Shell Nanocuboids Measured Experimentally (≈ 55 nm)

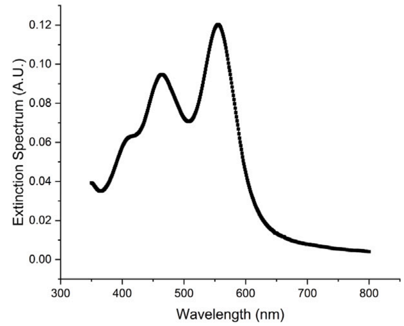

(b) Extinction Spectrum of Gold–Core Silver–Shell Nanocuboids Determined to be Optimal from the Simulations

Fig. 12. Experimentally measured extinction spectrum and extinction spectrum optimised via the model.

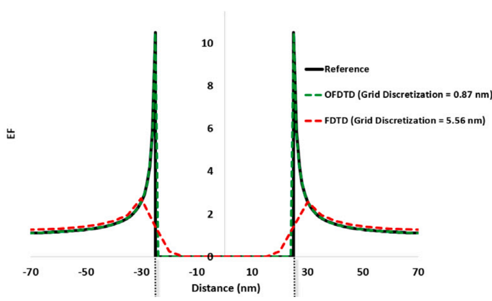

(a) PDEF Used in the Development and Optimisation of the Modelling Software

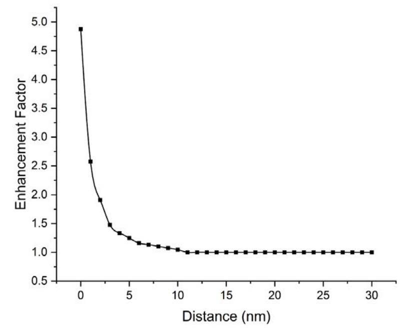

(b) Photon Density Enhancement Factor Altered for PLSC Model Validation

Fig. 13. Photon density enhancement factor used in model optimisation and the altered PDEF to match MNPs used in this study.

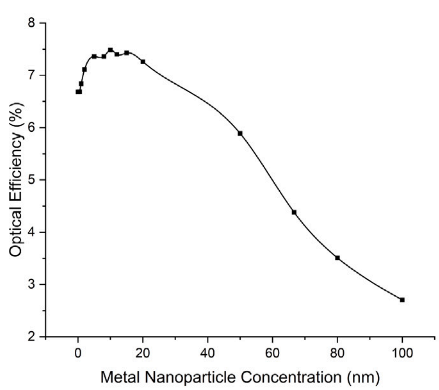

(a) Optical Efficiency vs Metal Nanoparticle Concentration Simulations

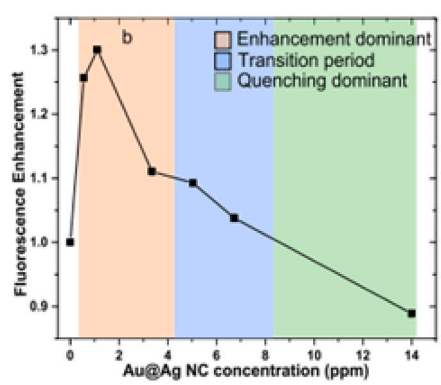

(b) Fluorescent Enhancement vs Metal Nanoparticle Concentration (Sethi et al., 2019)

Fig. 14. The effect of MNP concentration on device output in simulations and in experimental measurement.

development and validation of the newly developed electrical model. The results of the outdoor tests are included in Figs. 16 through 19. They display the devices' power output and power conversion efficiencies over four separate days of testing. As mentioned, when initially comparing the outdoor data with the models' predictions, it was noted that the simulation predictions were underestimating the power output and power conversion efficiencies when the environment was highly diffuse (>50%) and overestimating these metrics when the environment was highly direct (<5%). Data analysis found experimental coefficients of 1.76288 and 0.78665 for the highly diffuse and highly direct conditions respectively which is in line with a previous independent prediction observed through simulations using the optical model before validation as depicted in Fig. 15, where a factor of 1.76 is noted again when the diffuse component of the solar radiation spectrum is dominant. After correlating these findings, the factor has been built into the model to adjust its predictions across all datasets equally.

Figs. 16 & 17 display the simulated and experimental results in terms of electrical power outputs and power conversion efficiencies in

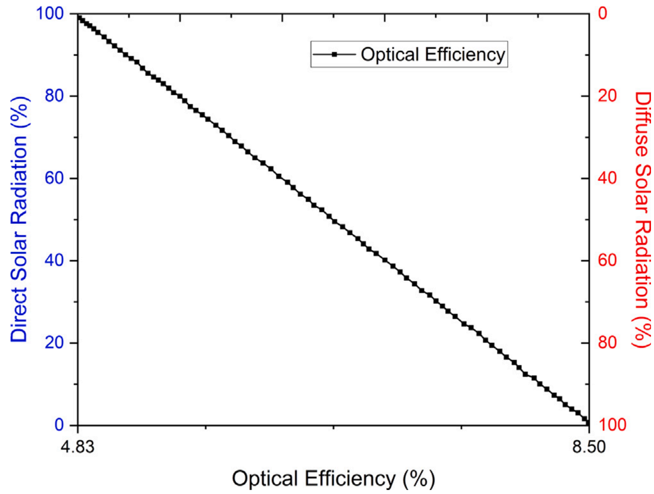

Fig. 15. Effect of the ratio of direct vs. Diffuse radiation on optical efficiency. *Source:* Adapted from [33].

quite overcast days in which the solar radiation reaches a maximum of 300 W/m^2. Figs. 18 & 19 detail these same result types on other days where the direct component of the solar radiation spectrum is more dominant with the maximum solar radiation reaching almost 800 W/m^2.

After analysing these datasets, the novel electrical part of the model has also been deemed validated due to its high degree of accuracy in predicting the performance of the LSC devices particularly in terms of their power outputs under various solar radiation conditions outdoors. The model predictions for the devices' power outputs were over 90% accurate in 3 out of 4 days, only on the 20th was it closer to 50% accurate and this is largely due to the noise in the data likely caused by a temporary obstruction to the pyranometer. The model is also accurate at predicting the power conversion efficiencies of the devices' but is let down during the beginning and end of the days when solar radiation is especially low. This finding correlates with another finding which states that the four–probe connection struggles with solar radiation less than 120 W/m^2 [44]. The low overall accuracy of between 20%–45% here is largely due to these differences at the start and ends of the graphs as they reach accuracies between 70%–90% when these tail ends are excluded. All of these congruence calculations have been performed using regression analysis on RStudio software.

This study has therefore validated an all encompassing optical and electrical model which can simulate the LSC & PLSC technologies and predict their outputs in various environments. The only specific experimental data required for this prediction is the local solar radiation spectrum separated into its direct and diffuse components and it will predict the power output and power conversion efficiencies.

4. Conclusion

This study presents and validates a novel two-stage integrated model capable of simulating both the optical and electrical outputs of Luminescent Solar Concentrators (LSCs) and Plasmonic Luminescent Solar Concentrators (PLSCs). The model's accuracy was initially established through comparisons between simulations and experimental data obtained from LSCs fabricated in the laboratory. Subsequently, the validation was extended to PLSCs by incorporating additional data related to gold–core silver–shell nanocuboid metal nanoparticles (MNPs). The high congruence between simulation and experimental results in both indoor and outdoor environments confirmed the model's reliability.

Following the validation of the optical model, simulations were utilised to enhance the performance of the LSC devices by determining an optimal LSC dimension, PV cell configuration, and doping concentration for the dye to maximise the optical efficiency and solar concentration ratio of the device. These optimised devices were fabricated and tested in both indoor and outdoor environments. These experimental results were then compared with the second –stage electrical model's predictions and the model was declared validated due to its high degree of accuracy (>90%) at predicting the device outputs.

This comprehensive model is capable of simulating real–world performance of LSC & PLSC devices using only the solar radiation data of a specific location and the devices' characteristics (dye absorption & emission, host matrix material, device dimensions and refractive index). The validated model has the ability to accurately simulate both the optical and electrical processes within LSC and PLSC devices. This model can be used with only manufacturers data on dye and MNPs to predict real-world performance for various device configurations using only solar radiation data and device configuration details. This comprehensive model offers significant material, time, and cost savings by reducing the need for repeated experimental testing.

In summary, this study has developed a powerful and versatile tool for LSC and PLSC research and development. The outcome is a verified model capable of simulating various device configurations, dimensions, dye types and concentrations, as well as different metal nanoparticle types and concentrations in area specific conditions in terms of both their optical characteristics as well as their outdoor electrical performance. The model's capabilities promises to advance the efficiency and practicality of solar concentrator technologies, contributing to the broader goal of enhancing renewable energy solutions.

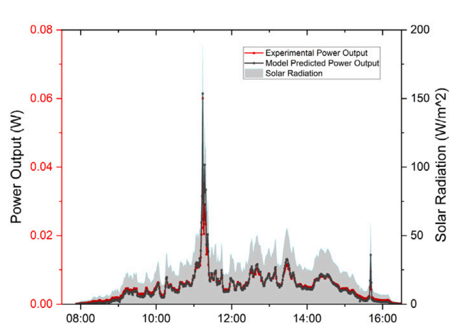

(a) Experimental and Model Predicted Power Output Comparisons

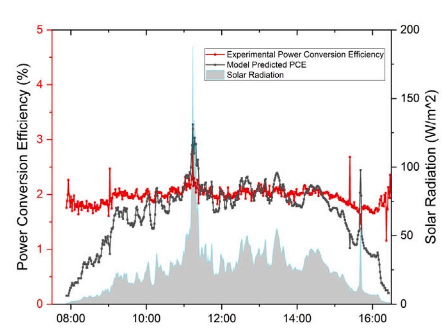

(b) Experimental and Model Predicted Power Conversion Efficiency Comparisons

Fig. 16. Experimental and Simulation results for the 13th of November, the congruence is 97.7% and 43.7% for the power output and power conversion efficiency predictions respectively.

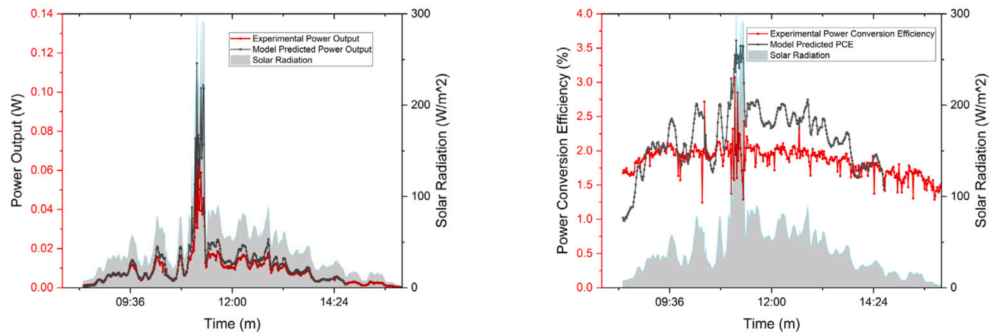

(a) Experimental and Model Predicted Power Output Comparisons

(b) Experimental and Model Predicted Power Conversion Efficiency Comparisons

Fig. 17. Experimental and Simulation results for the 17th of November, the congruence is 91.7% and 20.4% for the power output and power conversion efficiency predictions respectively.

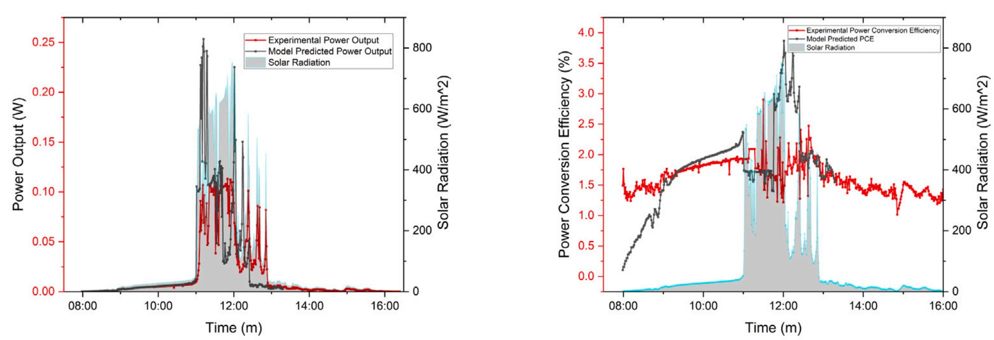

(a) Experimental and Model Predicted Power Output Comparisons

(b) Experimental and Model Predicted Power Conversion Efficiency Comparisons

Fig. 18. Experimental and Simulation results for the 20th of November, the congruence is 46.1% and 20.4% for the power output and power conversion efficiency predictions respectively.

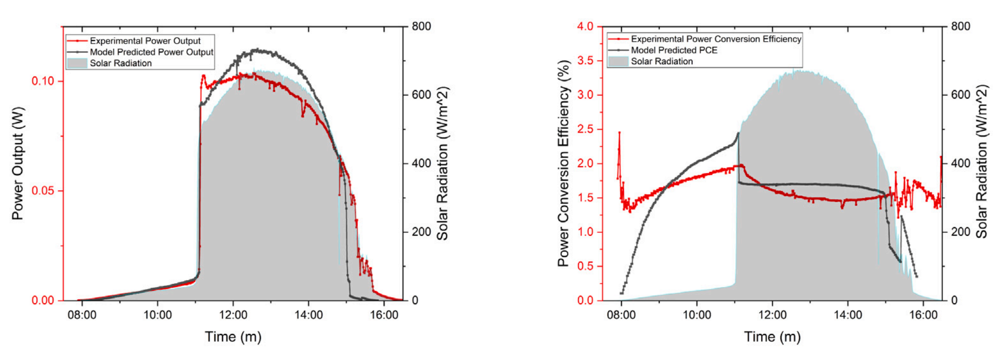

(a) Experimental and Model Predicted Power Output Comparisons

(b) Experimental and Model Predicted Power Conversion Efficiency Comparisons

Fig. 19. Experimental and Simulation results for the 21st of November, the congruence is 90.7% and 18.3% for the power output and power conversion efficiency predictions respectively.

CRediT authorship contribution statement

Aaron Glenn: Writing – review & editing, Writing – original draft, Methodology, Investigation, Formal analysis, Data curation. **Subhash Chandra:** Writing – review & editing, Supervision. **Mojtaba Nasiri:** Software. **Sarah McCormack:** Writing – review & editing, Supervision, Resources, Funding acquisition.

Declaration of competing interest

The authors declare that they have no known competing financial interests or personal relationships that could have appeared to influence the work reported in this paper.

Acknowledgements

This research work was funded by European research council under the project Plasmonic Enhancement and Directionality of Emission for Advanced Luminescent Solar Devices (PEDAL Project: 639760) and European Union funded Horizon 2020 project Novel building Integration Designs for increased Efficiencies in Advanced climatically tunable renewable energy Systems (IDEAS Project: 815271). The authors would also like to acknowledge Science Foundation Ireland (SFI) and ERC Evolute for research infrastructure.

References

[1] H. Ritchie, M. Roser, P. Rosado, Carbon dioxide and greenhouse gas emissions, Our World Data (2020) https://ourworldindata.org/co2-and-greenhouse-gas-emissions.

[2] A. Mikhaylov, N. Moiseev, K. Aleshin, T. Burkhardt, Global climate change and greenhouse effect, Entrepreneurship Sustain. Issues 7 (4) (2020) 2897–2913, http://dx.doi.org/10.9770/jesi.2020.7.4(21).

[3] S. Montzka, E. Dlugokencky, J. Butler, Non-CO2 greenhouse gases and climate change, Nature 476 (2011) 43–50, http://dx.doi.org/10.1038/nature10322.

[4] T.S. Ledley, E.T. Sundquist, S.E. Schwartz, D.K. Hall, J.D. Fellows, T.L. Killeen, Climate change and greenhouse gases, EOS Trans. Am. Geophys. Union 80 (39) (1999) 453–458, http://dx.doi.org/10.1029/99EO00325, arXiv:https://agupubs.onlinelibrary.wiley.com/doi/pdf/10.1029/99EO00325. URL https://agupubs.onlinelibrary.wiley.com/doi/abs/10.1029/99EO00325.

[5] NASA, Carbon dioxide vital signs, 2024, URL https://climate.nasa.gov/vital-signs/carbon-dioxide/?intent=121. (Accessed 05 June 2024).

[6] EESI, Fossil fuels, environmental and energy study institute, 2021, https://www.eesi.org/topics/fossil-fuels/description#:~:text=Fossil%20fuels%E2%80%94including%20coal%2C%20oil,percent%20of%20the%20world's%20energy.

[7] Z.H.P. Friedlingstein, Analysis: Global CO2 emissions from fossil fuels hits record high in 2022, World Econ. Forum (WEF) (2022) URL https://www.weforum.org/agenda/2022/11/global-co2-emissions-fossil-fuels-hit-record-2022.

[8] European Commission, In focus: Energy efficiency in buildings, 2020, https://commission.europa.eu/news/focus-energy-efficiency-buildings-2020-02-17_en. (Accessed 13 May 2024).

[9] S.M. Jordaan, E. Romo-Rabago, R. McLeary, L. Reidy, J. Nazari, I.M. Herremans, The role of energy technology innovation in reducing greenhouse gas emissions: A case study of Canada, Renew. Sustain. Energy Rev. 78 (2017) 1397–1409, http://dx.doi.org/10.1016/j.rser.2017.05.162, URL https://www.sciencedirect.com/science/article/pii/S1364032117307700.

[10] N. Panwar, S. Kaushik, S. Kothari, Role of renewable energy sources in environmental protection: A review, Renew. Sustain. Energy Rev. 15 (3) (2011) 1513–1524, http://dx.doi.org/10.1016/j.rser.2010.11.037, URL https://www.sciencedirect.com/science/article/pii/S1364032110004065.

[11] P.A. Østergaard, N. Duic, Y. Noorollahi, H. Mikulcic, S. Kalogirou, Sustainable development using renewable energy technology, Renew. Energy 146 (2020) 2430–2437, http://dx.doi.org/10.1016/j.renene.2019.08.094, URL https://www.sciencedirect.com/science/article/pii/S0960148119312819.

[12] N. National Renewable Energy Laboratory, Life cycle assessment harmonization, Sustain. Anal. (2023) URL https://www.nrel.gov/analysis/life-cycle-assessment.html.

[13] I. Sychugov, Analytical description of a luminescent solar concentrator, Optica 6 (8) (2019) 1046–1049, http://dx.doi.org/10.1364/OPTICA.6.001046, URL https://opg.optica.org/optica/abstract.cfm?URI=optica-6-8-1046.

[14] A. Kerrouche, D. Hardy, D. Ross, B. Richards, Luminescent solar concentrators: From experimental validation of 3D ray-tracing simulations to coloured stained-glass windows for BIPV, Sol. Energy Mater. Sol. Cells 122 (2014) 99–106, http://dx.doi.org/10.1016/j.solmat.2013.11.026, URL https://www.sciencedirect.com/science/article/pii/S0927024813006107.

[15] A.J. Chatten, K.W.J. Barnham, B.F. Buxton, N.J. Ekins-Daukes, M.A. Malik, Quantum dot solar concentrators, Semiconductors 38 (8) (2004) 909–917, http://dx.doi.org/10.1134/1.1787111.

[16] S. Chandra, J. Doran, S. McCormack, M. Kennedy, A. Chatten, Enhanced quantum dot emission for luminescent solar concentrators using plasmonic interaction, Sol. Energy Mater. Sol. Cells 98 (2012) 385–390, http://dx.doi.org/10.1016/j.solmat.2011.11.030, URL https://www.sciencedirect.com/science/article/pii/S0927024811006441.

[17] J. Day, S. Senthilarasu, T.K. Mallick, Enhanced efficiency for building integrated concentrator photovoltaic modules based on rare earth doped optics, Sol. Energy Mater. Sol. Cells 199 (2019) 83–90, http://dx.doi.org/10.1016/j.solmat.2019.04.013, URL https://www.sciencedirect.com/science/article/pii/S0927024819301904.

[18] A. Glenn, S. Chandra, S. McCormack, Design, fabrication and preliminary testing of plasmonic luminescent solar concentrator devices, Innov. Technol. Integr. Syst. High Perform. Build. Sustain. Build. 6 (8) (2023) http://dx.doi.org/10.1051/sbuild/2023009.

[19] W.H. Weber, J. Lambe, Luminescent greenhouse collector for solar radiation, Appl. Opt. 15 (10) (1976) 2299–2300, http://dx.doi.org/10.1364/AO.15.002299, URL https://opg.optica.org/ao/abstract.cfm?URI=ao-15-10-2299.

[20] M. Kennedy, S. McCormack, J. Doran, B. Norton, Improving the optical efficiency and concentration of a single-plate quantum dot solar concentrator using near infra-red emitting quantum dots, Sol. Energy 83 (7) (2009) 978–981, http://dx.doi.org/10.1016/j.solener.2008.12.010, URL https://www.sciencedirect.com/science/article/pii/S0038092X08003484.

[21] K. Barnham, J.L. Marques, J. Hassard, P. O'Brien, Quantum-dot concentrator and thermodynamic model for the global redshift, Appl. Phys. Lett. 76 (9) (2000) 1197–1199, http://dx.doi.org/10.1063/1.125981, arXiv:https://pubs.aip.org/aip/apl/article-pdf/76/9/1197/10185114/1197_1_online.pdf.

[22] O. Essahili, M. Ouafi, O. Moudam, Recent progress in organic luminescent solar concentrators for agrivoltaics: Opportunities for rare-earth complexes, Sol. Energy 245 (2022) 58–66, http://dx.doi.org/10.1016/j.solener.2022.08.054, URL https://www.sciencedirect.com/science/article/pii/S0038092X22006041.

[23] P. Barik, M. Pradhan, Plasmonic luminescent solar concentrator, Sol. Energy 216 (2021) 61–74, http://dx.doi.org/10.1016/j.solener.2021.01.018, URL https://www.sciencedirect.com/science/article/pii/S0038092X21000347.

[24] A. Sethi, S. Chandra, A. Ortega, S. McCormack, Outdoor characterization of a plasmonic luminescent solar concentrator, Plasmonics 17 (2) (2022) 725–734, http://dx.doi.org/10.1007/s11468-021-01562-y.

[25] N. Harris, M.G. Blaber, G.C. Schatz, Optical properties of metal nanoparticles, in: Encyclopedia of Nanotechnology, Springer Netherlands, Dordrecht, 2016, pp. 3027–3048, http://dx.doi.org/10.1007/978-94-017-9780-1_22.

[26] J.P. Nolan, D.S. Sebba, Chapter 20 - surface-enhanced Raman scattering (SERS) cytometry, in: Z. Darzynkiewicz, E. Holden, A. Orfao, W. Telford, D. Wlodkowic (Eds.), Recent Advances in Cytometry, Part a, in: Methods in Cell Biology, vol. 102, Academic Press, 2011, pp. 515–532, http://dx.doi.org/10.1016/B978-0-12-374912-3.00020-1, URL https://www.sciencedirect.com/science/article/pii/B9780123749123000201.

[27] M. Rycenga, C.M. Cobley, J. Zeng, W. Li, C.H. Moran, Q. Zhang, D. Qin, Y. Xia, Controlling the synthesis and assembly of silver nanostructures for plasmonic applications, Chem. Rev. 111 (6) (2011) 3669–3712, http://dx.doi.org/10.1021/cr100275d.

[28] N. Chandrasekharan, P.V. Kamat, Improving the photoelectrochemical performance of nanostructured TiO2 films by adsorption of gold nanoparticles, J. Phys. Chem. B 104 (46) (2000) 10851–10857, http://dx.doi.org/10.1021/jp0010029.

[29] A. Chatten, D. Farrel, C. Jermyn, P. Thomas, B. Buxton, A. Buchtemann, R. Danz, K. Barnham, Thermodynamic modelling of luminescent solar concentrators, in: Conference Record of the Thirty-First IEEE Photovoltaic Specialists Conference, 2005., 2005, pp. 82–85, http://dx.doi.org/10.1109/PVSC.2005.1488074.

[30] Á. Bognár, S. Kusnadi, L.H. Slooff, C. Tzikas, R.C. Loonen, M.M. de Jong, J.L. Hensen, M.G. Debije, The solar noise barrier project 4: Modeling of full-scale luminescent solar concentrator noise barrier panels, Renew. Energy 151 (2020) 1141–1149, http://dx.doi.org/10.1016/j.renene.2019.11.102, URL https://www.sciencedirect.com/science/article/pii/S0960148119317951.

[31] S. Verma, D.J. Farrell, R.C. Evans, Ray-trace modeling to characterize efficiency of unconventional luminescent solar concentrator geometries, ACS Appl. Opt. Mater. 1 (5) (2023) 1012–1025, http://dx.doi.org/10.1021/acsaom.3c00074.

[32] M.G. Debije, R.C. Evans, G. Griffini, Laboratory protocols for measuring and reporting the performance of luminescent solar concentrators, Energy Environ. Sci. 14 (2021) 293–301, http://dx.doi.org/10.1039/D0EE02967J.

[33] M. Rafiee, 3D Modelling Tool to Optimise Advanced Plasmonic Luminescent Solar Devices for Building Integrated Photovoltaic Applications (Ph.D. thesis), Trinity College Dublin, 2019.

[34] P. André, L. Dias, S. Correia, A. Carneiro Neto, R. Ferreira, Artificial neural networks for predicting optical conversion efficiency in luminescent solar concentrators, Sol. Energy 268 (2024) 112290, http://dx.doi.org/10.1016/j.solener.2023.112290, URL https://www.sciencedirect.com/science/article/pii/S0038092X23009246.

[35] A. Glenn, S. Chandra, M. Nasiri, A. Ortega, S.J. McCormack, Fabrication and performance evaluation of large–scale luminescent and plasmonic luminescent solar concentrator modules, Sol. Energy 282 (2024) 112972, http://dx.doi.org/10.1016/j.solener.2024.112972, URL https://www.sciencedirect.com/science/article/pii/S0038092X24006674.

[36] K. Yee, Numerical solution of initial boundary value problems involving Maxwell's equations in isotropic media, IEEE Trans. Antennas and Propagation 14 (3) (1966) 302–307, http://dx.doi.org/10.1109/TAP.1966.1138693.

[37] A. Iserles, Generalized leapfrog methods, IMA J. Numer. Anal. 6 (4) (1986) 381–392, http://dx.doi.org/10.1093/imanum/6.4.381, arXiv:https://academic.oup.com/imajna/article-pdf/6/4/381/2181277/6-4-381.pdf.

[38] A. Sethi, S. Chandra, H. Ahmed, S. McCormack, Broadband plasmonic coupling and enhanced power conversion efficiency in luminescent solar concentrator, Sol. Energy Mater. Sol. Cells 203 (2019) 110150, http://dx.doi.org/10.1016/j.solmat.2019.110150, URL https://www.sciencedirect.com/science/article/pii/S0927024819304799.

[39] A. Glenn, S. Chandra, S. McCormack, Validation of plasmonic luminescent solar concentrator modelling software, in: Advanced Modeling and Characterization, the 8th World Conference on Photovoltaic Energy Conversion, 2BV.2.53, The 8th World Conference on Photovoltaic Energy Conversion, 2022, pp. 457–461, http://dx.doi.org/10.4229/WCPEC-82022-2BV.2.53.

[40] B. Nikoobakht, M.A. El-Sayed, Preparation and growth mechanism of gold nanorods (NRs) using seed-mediated growth method, Chem. Mater. 15 (10) (2003) 1957–1962, http://dx.doi.org/10.1021/cm020732l.

[41] L. Scarabelli, A. Sánchez-Iglesias, J. Pérez-Juste, L.M. Liz-Marzán, A "Tips and Tricks" practical guide to the synthesis of gold nanorods, J. Phys. Chem. Lett. 6 (21) (2015) 4270–4279, http://dx.doi.org/10.1021/acs.jpclett.5b02123.

[42] R. Thomas, J. Kumar, R. Swathi, K. Thomas, Optical effects near metal nanostructures: Towards surface-enhanced spectroscopy, Current Sci. 102 (2012) 85–96.

[43] M. Aghaei, M. Nitti, N.J. Ekins-Daukes, A.H. Reinders, Simulation of a novel configuration for luminescent solar concentrator photovoltaic devices using bifacial silicon solar cells, Appl. Sci. 10 (3) (2020) 871, http://dx.doi.org/10.3390/app10030871.

[44] M.S. National Renewable Energy Laboratory, J. Polo, C. Gueymard, Y. Xie, Best practices handbook for the collection and use of solar resource data for solar energy applications: Third edition, 2021, URL https://www.nrel.gov/docs/fy21osti/77635.pdf.